2019 IEEE/RSJ International Conference on Intelligent Robots and Systems (IROS)
Macau, China, November 4-8, 2019

A Dynamic Optimization Approach for Sloshing Free Transport of Liquid Filled Containers using an Industrial Robot

Jan Reinhold, Manuel Amersdorfer, *Student Member, IEEE* and Thomas Meurer, *Senior Member, IEEE*

***Abstract*— The handling of liquid filled containers is a challenging task in industrial manufacturing processes. Without an appropriate trajectory sloshing of the liquid occurs during point-to-point motion. This paper presents a time optimal trajectory planning approach that is used for feedforward motion control and prevents the liquid filled container from sloshing. For this, a model of the liquid inside the container is included into the formulation of a constrained dynamic optimization problem to achieve rest-to-rest motion while simultaneously avoiding obstacles. The presented approach is validated by simulation and on an experimental setup using an industrial robot handling the container.**

I. INTRODUCTION

Industrial production and manufacturing processes involve complex transport and processing operations that progressively rely on the integration of suitable automation measures and robot assistance systems. One particular task in this context, that arises, e.g., in food and pharmaceutical industries, is the handling of liquid filled objects. This becomes increasingly complex for fast handling operations where undesired sloshing and even spilling out of the liquid may appear during motion and transport. For heavy liquid filled containers sloshing induces stress on the handling structure and may induce unexpected behavior even under closed-loop control operation if the sloshing dynamics are not considered in the control design.

Taking into account models of the sloshing dynamics closed-loop approaches allow to achieve rather robust sloshing suppression, see, e.g., [1]–[4] and the references therein. Feedback control, however, relies on the acquisition and real-time processing of suitable sensor data and hence requires containers equipped with appropriate sensors and signal processing units, which is in many situations not applicable or feasible.

Alternatively, feedforward control methods can be used to determine the input signal to the system to realize the desired container motion with minimal sloshing considering a given reference trajectory. Examples include the application of input shaping or feedforward vibration suppression [5]–[9]. One disadvantage of these methods is that acceleration and deceleration trajectories of the container need to be determined that either prevent the excitation of the sloshing dynamics in open-loop (corresponding to slow motion and long transfer times) or that require the compensation of the sloshing wave by superimposing appropriate signals (corresponding to availability of accurate parametrized models).

The authors are with the Chair of Automatic Control, Faculty of Engineering, Kiel University, Kaiserstraße 2, 24143 Kiel, Germany, {janr,maam,tm}@tf.uni-kiel.de

It should be noted that in most feedforward approaches, see, e.g., [5]–[9] the container is kept upright during the point-to-point motion. However, examining a human while manually moving a liquid filled cup exposes swaying and rotating motion of the hand and the wrist to attenuate the liquid's motion. This intuitive approach pursues the strategy to tilt the cup so that relative motion between liquid and cup is avoided during acceleration and deceleration. In [10] a plugin feedforward control with an active compensation of lateral accelerations is introduced by modifying the container orientation. In other previous works, a related strategy was realized by using suitable feedback control [11], [12].

The present paper deals with an approach, which enables the sloshing free transfer of a liquid filled container in minimum time using feedforward control. Therefore, the trajectory planning task is formulated as an optimal control problem for the translational and rotational point-to-point motion of the container from an initial to a terminal steady state. In addition, static and dynamic constraints can be included into the problem setting. In contrast to [13] the application of the resulting feedforward control as optimal input trajectory leads to an orientation of the container aligned with the liquid surface during the motion. Moreover, the relative motion between the liquid and the container is minimized, hence preventing sloshing while the whole transfer. This strategy can also be generalized to other transport problems such as handling of unsecured stacked loads.

The Section II addresses the modelling of the liquid inside the container. Planning of the time optimal trajectory in the three dimensional space is discussed in Section III. The approach is extended to prevent the container from collisions with obstacles. Experimental and simulation results are presented in Section IV. Section V concludes the paper and discusses future extensions of the presented methods.

II. MODELING

The sloshing free transport of a liquid filled container in the three dimensional space using model based trajectory planning requires a mathematical model of the transport system and the dynamics of the liquid during motion. The proposed experimental setup in Fig. 1 uses a robotic manipulator, where a tank containing the transported liquid is mounted at the end-effector. The base of the manipulator represents the origin of the initial frame, where the horizontal plane is spanned by the x_0- and y_0-axes and the z_0-axis describes the vertical direction. The origin of the container frame, denoted by the index c, is located at the surface of the

978-1-7281-4004-9/19/$31.00 ©2019 IEEE

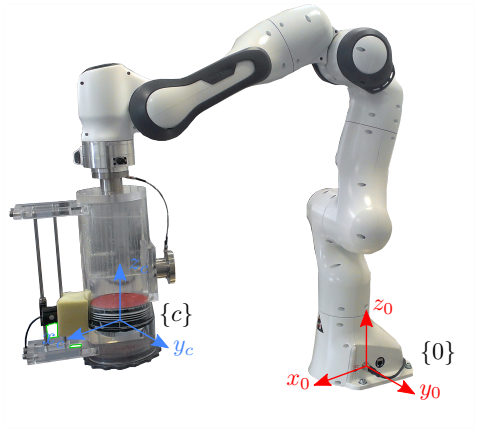

Fig. 1. Utilized manipulator with mounted liquid filled container.

liquid in steady state. The manipulator's end-effector pose

$$\boldsymbol{x}_0^c = \begin{bmatrix} \boldsymbol{p}_0^c \\ \boldsymbol{\phi}_0^c \end{bmatrix} = \boldsymbol{k}(\boldsymbol{q}) \tag{1}$$

includes the end-effector position $\boldsymbol{p}_0^c = [x_0^c\ y_0^c\ z_0^c]^{\mathrm{T}}$ and the Euler-angles $\boldsymbol{\phi}_0^c = [\phi_0^c\ \theta_0^c\ \psi_0^c]^{\mathrm{T}}$ describing the rotation matrix R_0^c of the container with respect to the initial frame. The function $\boldsymbol{k}(\boldsymbol{q})$ denotes the forward kinematics of the robot with generalized coordinates $\boldsymbol{q} \in \mathbb{R}^n$ including the rotation angles of the n joints [14]. To satisfy the full agibility of the end-effector in the task space the condition $n \geq 6$ has to hold. Subsequently, the sloshing dynamics inside the container is addressed: at first for one-dimensional and secondly for three-dimensional container motion trajectories.

A. One-Dimensional Container Sloshing Dynamics

As described in [15] the sloshing of a liquid is caused by an oscillatory motion of the liquid transporting kinetic energy and can be expressed by the shallow-water equations. In [15], it is shown that the sloshing effect can be modelled by an equivalent mechanical model, e.g., a spring mass system or a pendulum.

To connect the effect of sloshing to the orientation of the liquid's surface inside the container, subsequently the model of a single mode damped pendulum is used, by assuming that the wavelength of liquid waves is much smaller than the tank diameter. The pendulum visualized in Fig. 2 involves the angle φ describing the rotation between the surface normal of the liquid in the body fixed coordinate system $\{l\}$ relative to the initial frame $\{0\}$. The time derivative $\dot{\varphi}$ describes the rotational velocity of the pendulum. We consider the translational acceleration $\ddot{y}_0$ in y_0-direction generated by the robot manipulator as external input u to the system independent of the position of the container in the task space. The mass m of the pendulum is assumed to rotate with the distance l around to the x_0-axis. The interaction between the liquid and the container borders is assumed to damp the liquid's motion. This is represented in the model by the dashpot with the damping constant d.

The equations of motion of the damped pendulum representation of Fig. 2 can be determined by applying the Euler-Lagrange formalism, which yields

$$\ddot{\varphi} = \frac{u}{l}\cos(\varphi) - \frac{g}{l}\sin(\varphi) - \frac{d}{m}\,\dot{\varphi}\cos^2(\varphi) \tag{2}$$

for $t > t_0$ with the inital conditions $\varphi(t_0) = \varphi_0$, $\dot{\varphi}(t_0) = \dot{\varphi}_0$. Here, $g = 9.81\,\mathrm{m\,s^{-2}}$ is the gravitational constant.

B. Three-Dimensional Container Sloshing Dynamics

The one-dimensional pendulum abstraction of the sloshing dynamics in terms of (2) can be generalized to describe the corresponding behaviour in three-dimensional space. For this, the motion of the container and the liquid can be split into horizontal and vertical components depending on the acceleration $\boldsymbol{u} = [u_x\ u_y\ u_z]^{\mathrm{T}}$ of the container imposed by the robot manipulator.

The influence of the vertical acceleration u_z on the sloshing behaviour is considered by subtracting it from the gravity acceleration g in (2). As shown in [16] this impact can be neglected for sufficiently small vertical accelerations. In [8], [9], [12] model couplings the x_0- and y_0-direction are considered to represent the sloshing dynamics for horizontal motion, which, however, increases the calculation complexity and assumes a symmetric container shape. Contrary, in the following the two motion directions are considered independently taking into account (2) and the resulting sloshing motion is given as the superposition of the two orthogonal contributions. This assumption is confirmed by our experimental results and enables us to extend our approach also to certain unsymmetric container geometries.

The pose $\boldsymbol{x}_0^l = [(\boldsymbol{p}_0^l)^{\mathrm{T}}\ (\boldsymbol{\phi}_0^l)^{\mathrm{T}}]^{\mathrm{T}}$, where $\boldsymbol{p}_0^l = [x_0^l\ y_0^l\ z_0^l]^{\mathrm{T}}$ describes the position of the center of the liquid's surface and $\boldsymbol{\phi}_0^l = [\phi_0^l\ \theta_0^l\ \psi_0^l]^{\mathrm{T}}$ the orientation of the liquid relative to the initial coordinate system. Considering these relationships, the three-dimensional liquid dynamics in Cartesian coordinates

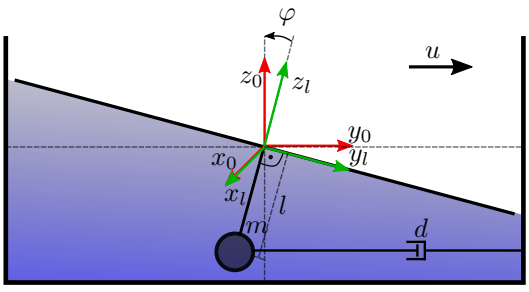

Fig. 2. Representing the liquid inside the container as a single, damped pendulum with length l, mass m, damping constant d, rotation angle φ, and translational acceleration u. The coordinate system $\{l\}$ (green) is aligned with the surface of the liquid while $\{0\}$ (red) is parallel to the initial frame.

is governed by

$$\frac{\mathrm{d}}{\mathrm{d}t}\underbrace{\begin{bmatrix} x_0^l \\ y_0^l \\ z_0^l \\ \phi_0^l \\ \theta_0^l \\ \psi_0^l \\ \dot{x}_0^l \\ \dot{y}_0^l \\ \dot{z}_0^l \\ \dot{\phi}_0^l \\ \dot{\theta}_0^l \\ \dot{\psi}_0^l \end{bmatrix}}_{=\boldsymbol{o}_0^l} = \underbrace{\begin{bmatrix} \dot{x}_0^l \\ \dot{y}_0^l \\ \dot{z}_0^l \\ \dot{\phi}_0^l \\ \dot{\theta}_0^l \\ \dot{\psi}_0^l \\ u_x \\ u_y \\ u_z \\ \frac{u_y}{l_\phi}\cos\phi_0^l - \frac{g-u_z}{l_\phi}\sin\phi_0^l - \frac{d_\phi}{m}\dot{\phi}_0^l\cos^2\phi_0^l \\ \frac{u_x}{l_\theta}\cos\theta_0^l - \frac{g-u_z}{l_\theta}\sin\theta_0^l - \frac{d_\theta}{m}\dot{\theta}_0^l\cos^2\theta_0^l \\ 0 \end{bmatrix}}_{=\boldsymbol{f}\left(\boldsymbol{o}_0^l,\,\boldsymbol{u}\right)} \tag{3}$$

with $\boldsymbol{o}_0^l = [(\boldsymbol{x}_0^l)^\mathrm{T}\ (\dot{\boldsymbol{x}}_0^l)^\mathrm{T}]^\mathrm{T}$. Herein, $\dot{\psi}_0^l = 0$ implies that no rotation around the z_0-axis occurs. The index $\{l\}$ refers to the frame aligned with the liquid surface relative to the initial frame. The parameters l_ϕ, d_ϕ, l_θ, and d_θ in particular depend on the container geometry and are determined subsequently.

C. Parameter Identification

In the following, a cylindrical container is considered, so that $d = d_\phi = d_\theta$ and $l = l_\phi = l_\theta$ can be assumed. The mass $m = \rho^l V$ is given by the container volume V and the liquid density ρ^l. For the determination of the model parameters l and d based on (2) we consider the linearized equations of motion around the stable steady state $\varphi = 0$, i.e.,

$$\ddot{\varphi} + \frac{d}{m}\,\dot{\varphi} + \frac{g}{l}\,\varphi = \frac{u}{l}. \tag{4}$$

This is in rather good accordance with physical evidence for moderate accelerations $\boldsymbol{u}$ of the container. By making use of the Laplace transform $\mathcal{L}$ we obtain the transfer function

$$H(s) = \frac{\mathcal{L}(\varphi)}{\mathcal{L}(u)} = \frac{\frac{1}{g}}{\frac{l}{g}\,s^2 + \frac{d\,l}{g\,m}\,s + 1}. \tag{5}$$

Taking into account that (5) corresponds to a PT_2 element, whose transfer function

$$G(s) = \frac{K}{\frac{1}{\omega^2}\,s^2 + \frac{2\,\zeta}{\omega}\,s + 1} \tag{6}$$

can be written in terms of the magnitude K, the natural frequency ω and the dimensionless damping factor ζ the termwise comparison provides

$$\omega = 2\pi f = \sqrt{\frac{g}{l}}, \quad \zeta = \frac{d}{2m\omega}.$$

TABLE I

IDENTIFIED VALUES OF THE LIQUID PARAMETERS.

Parameter	Value	Unit
Mass of liquid, m	0.5	kg
Pendulum length, $l_\phi = l_\theta$	0.021	m
Damping constant, $d_\phi = d_\theta$	1.51	$\mathrm{N\,s\,m^{-1}}$

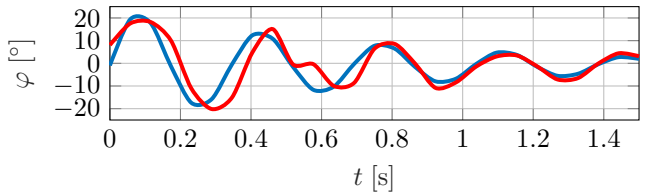

Fig. 3. Experimental impulse-like response of the liquid (red) compared to the impulse response (7) of a PT_2 element (blue).

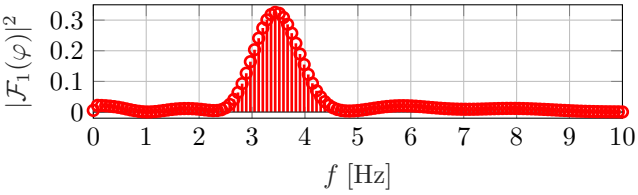

Fig. 4. Power spectral density of an one-sided Fourier transformation seperated with Hamming window of the measured sloshing angle φ of the liquid's impulse response.

For the determination of l, d or ω, ζ, respectively, we consider the response of the experimental container device shown in Fig. 1 to an impulse-like excitation. The sloshing motion is measured optically using a float swaying with the liquid's surface, see Fig. 3. Applying the Fourier transformation to the resulting signal yields the power spectral density shown in Fig. 4. This confirms the emergence of a single dominant mode and hence underlines the assumption of a single pendulum approximation of the sloshing motion.

After determining ω and hence l we make use of the analytical impulse response of a PT_2 element

$$\varphi = \frac{A}{\sqrt{1-\zeta^2}}\exp\left(-\zeta\omega t\right)\sin\left(\omega\sqrt{1-\zeta^2}\,t\right) \tag{7}$$

and minimize the least-squares error in ζ and hence d with respect to the experimental data (cf. Fig. 3). Here, the amplitude A is set to the absolute maximum of the measured impulse response. The identified values of the liquid parameters are listed in Tab. I.

III. TRAJECTORY PLANNING USING CONSTRAINED DYNAMIC OPTIMIZATION

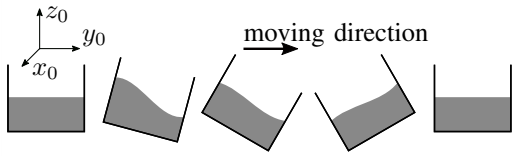

Fig. 5. Schematic scene of the container's orientation while one-dimensional transmission.

Utilizing the agility of the manipulator allows us to control the translational and rotational motion of the liquid filled container. This is used subsequently to achieve sloshing free point-to-point motion of the container. For the one-dimensional case addressed in Section II-A a schematic

motion diagram is shown in Fig. 5. It illustrates snapshots of the liquid container while moving in the y_0-direction under rotation around the perpendicular x_0-axis.

For trajectory planning and feedforward control we formulate and solve a constrained optimal control problem. Herein, the model of the liquid determined in Sections II-A and II-B, respectively, the velocity and acceleration limits of the robotic manipulator, as well as terminal conditions for the position and velocity of the system are taken into account.

A. Time Optimal Control Problem

To plan a sloshing-free transfer we consider the time optimal point-to-point motion of the liquid (3) from the initial state $\boldsymbol{o}_0^l(t_0) = \boldsymbol{o}_{0,\,0}^l$ to the terminal state $\boldsymbol{o}_0^l(t_1) = \boldsymbol{o}_{0,\,1}^l$. The planned trajectory describes the motion of the liquid during the transition in free space. The container mounted on the end-effector of the robot tracks the resulting state trajectory $\boldsymbol{o}_0^{l\,*}$ such that no relative motion between container and liquid occurs. For this, the control input in terms of the accelerations $\boldsymbol{u}$ imposed on the container by the robot manipulator serve as decision variables to solve the time optimal constrained minimization problem

$$\min_{\boldsymbol{u}\in\mathcal{U}} J(\boldsymbol{u}) = \int_{t_0}^{t_1} \left(1 + \frac{\kappa_r}{2}\,\|\boldsymbol{u}\|_2^2\right) \mathrm{d}t \tag{8a}$$

subject to

$$\dot{\boldsymbol{o}}_0^l = \boldsymbol{f}(\boldsymbol{o}_0^l,\, \boldsymbol{u}), \quad t > t_0 \tag{8b}$$

$$\boldsymbol{o}_0^l(t_0) = \boldsymbol{o}_{0,\,0}^l, \quad \boldsymbol{o}_0^l(t_1) = \boldsymbol{o}_{0,\,1}^l \tag{8c}$$

for a free end time t_1 and the set of admissible inputs

$$\mathcal{U} := \{\boldsymbol{u} \in \mathbb{R}^3 \mid -\boldsymbol{u}_{\max} \le \boldsymbol{u} \le \boldsymbol{u}_{\max}\}. \tag{8d}$$

The regularization term in (8a) with $0 < \kappa_r \ll 1$ is introduced to prevent the emergence of singular arcs. The input limits $\pm\boldsymbol{u}_{\max}$ follow from the robot dynamics and are given by the robot manufacturer. The free end time $t_1 = t_0 + T$ is limited by the translational distance and the maximum Cartesian velocity

$$\kappa_T\, \frac{\left\|\boldsymbol{p}_0^l(t_1) - \boldsymbol{p}_0^l(t_0)\right\|_2}{\|\dot{\boldsymbol{p}}_{0,\,\max}^l\|_2} \le T \tag{8e}$$

with $\kappa_T \ge 1$ to ensure a continuous optimal input trajectory. The states $\boldsymbol{o}_0^l$ of the system have to fulfill the state constraints

$$\begin{aligned} z_{0,\,\min}^l \le z_0^l \le z_{0,\,\max}^l \qquad & |\phi_0^l| \le \phi_{0,\,\max}^l \\ |\dot{x}_0^l| \le \dot{x}_{0,\,\max}^l \qquad & |\dot{\phi}_0^l| \le \dot{\phi}_{0,\,\max}^l \\ |\dot{y}_0^l| \le \dot{y}_{0,\,\max}^l \qquad & |\theta_0^l| \le \theta_{0,\,\max}^l \\ |\dot{z}_0^l| \le \dot{z}_{0,\,\max}^l \qquad & |\dot{\theta}_0^l| \le \dot{\theta}_{0,\,\max}^l \end{aligned} \tag{8f}$$

for all $t \in [t_0,\, t_1]$.

Solving (8) yields the optimal input trajectory $\boldsymbol{u}^*$ with the corresponding state trajectory $\boldsymbol{o}_0^{l\,*}$ of the system (3). In this work the numerical solution of (8) is obtained using the *Acado*-Toolkit [17] in terms of a multiple shooting method and a fourth order Runge-Kutta integrator.

Note that the states ϕ_0^l and θ_0^l describe the orientation of the liquid's surface with respect to the inital coordinate system. To ensure that the robot is able to track the planned optimal trajectory $\boldsymbol{o}_0^{l\,*}$ these angles and their time derivatives are constrained in (8f). A minimization of these states in (8a) would limit the rotational motion of the liquid but also increase the transition time T. By tracking the motion of the liquid with the end-effector of the robot it is ensured that no sloshing between the container and the liquid occurs, although the surface orientation of the liquid describes a motion relative to the inital coordinate system.

The optimal state trajectory $\boldsymbol{o}_0^{l\,*}$ can be split into a Cartesian pose trajectory $\boldsymbol{x}_0^{l\,*}$ and a Cartesian velocity trajectory $\dot{\boldsymbol{x}}_0^{l\,*}$. These trajectories are executed by a trajectory tracking controller of the robot. It is assumed that the bandwidth of this controller is much higher than the dynamics of the planned trajectory such that the relation for the desired Cartesian velocity $\dot{\boldsymbol{x}}_0^d = \dot{\boldsymbol{x}}_0^{l\,*}$ holds true.

B. Obstacle Avoidance

To address known static obstacles in the task space during the point-to-point motion the objective functional (8a) is extended according to

$$J(\boldsymbol{u}) = \int_{t_0}^{t_1} \left(1 + \frac{\kappa_r}{2}\,\|\boldsymbol{u}\|_2^2 + \kappa_B\, B\left(\boldsymbol{p}_0^l\right)\right) \mathrm{d}t \tag{9}$$

using the barrier function

$$B\left(\boldsymbol{p}_0^l\right) = -\sum_{k=1}^{K} \ln\!\left(\min\left\{1, \|\boldsymbol{p}_0^l - \boldsymbol{p}_0^k\|_2^2 - (r_0^k)^2\right\}\right) \tag{10}$$

with the weight $0 < \kappa_B$. This allows us to integrate spherical obstacles with the radius r_0^k centered at the point $\boldsymbol{p}_0^k = [x_0^k\, y_0^k\, z_0^k]^T$. Note that cylindrical obstacles or other obstacle geometries can be treated similarly.

IV. SIMULATION AND EXPERIMENT

The proposed approach is evaluated using the experimental setup shown in Fig. 1. The water filled cylindrical container is mounted on a 7-DOF robotic manipulator of type Franka EMIKA Panda [18]. To improve visibility the water in the container is colored with blue food colorant. The constrained optimal control problem introduced in Section III is solved on a separate PC that is connected to the robot controller.

A. One-Dimensional Point-to-Point Motion

The optimal state trajectory $\boldsymbol{o}_0^{l\,*}$ resulting from the dynamic optimization problem (8) is depicted in Fig. 6. The translational motion performs an one-dimensional point-to-point transition in y_0-direction connecting the initial steady state

$$\boldsymbol{o}_{0,\,0}^l = \begin{bmatrix} 0.3\,\mathrm{m} & -0.27\,\mathrm{m} & 0.2\,\mathrm{m} & \boldsymbol{0}^T \end{bmatrix}^T$$

and the terminal steady state

$$\boldsymbol{o}_{0,\,1}^l = \begin{bmatrix} 0.3\,\mathrm{m} & 0.27\,\mathrm{m} & 0.2\,\mathrm{m} & \boldsymbol{0}^T \end{bmatrix}^T$$

with distance $\Delta y_0^c = 0.54\,\mathrm{m}$. The orientation of the container follows the expected intuitive behavior, i.e. relative motion

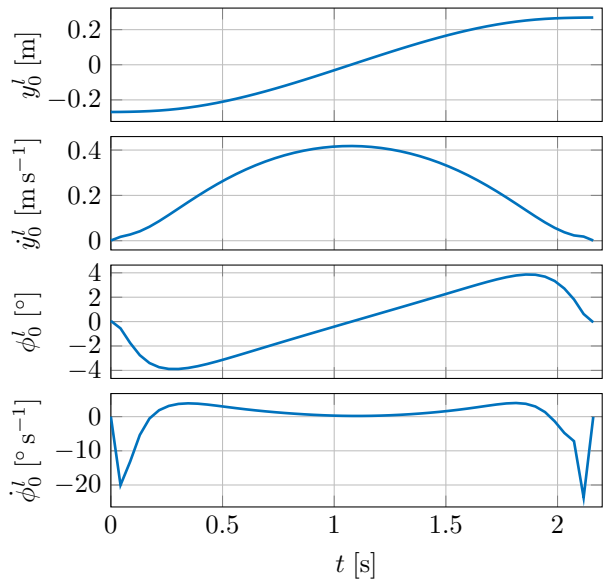

Fig. 6. Optimal state trajectory $\boldsymbol{o}_0^{l*}$ for one-dimensional sloshing free transfer by solving (8).

between container and liquid is avoided, as is illustrated in Fig. 5. It should be noticed that no information on the rotational behavior was given for the dynamic optimization problem except the model of the liquid. By using this robot the obtained minimal transition time is $T = t_1 - t_0 = 2.15\,\mathrm{s}$.

The motion of the liquid's surface is detected by measuring the angle of a float with a camera relative to the container. The optimal trajectory computed from (8) is executed using the Cartesian velocity controller of the robot with the desired Cartesian velocity trajectory $\dot{\boldsymbol{x}}_0^d = \dot{\boldsymbol{x}}_0^{l*} = [(\dot{\boldsymbol{p}}_0^{l*})^T\ (\dot{\boldsymbol{\phi}}_0^{l*})^T]^T$ from the velocity states of the optimal state trajectory $\boldsymbol{o}_0^{l*}$.

In Fig. 7 the measured sloshing angle with the proposed feedforward approach is shown and compared to a classical translational trajectory planning approach with constant acceleration and deceleration. It can be seen that the measured relative angle between container and the surface of the liquid stays at zero for the feedforward trajectory. Contrary the measurements obtained for the classical translational trajectory planning approach show large deviations caused by the motion-induced sloshing of the liquid.

For better visualization the reader is referred to [19], where a video of the experiment results is provided that compares the behavior of the liquid-filled container with the proposed

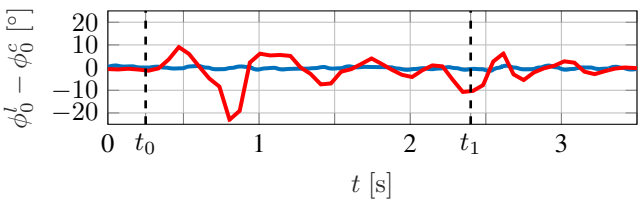

Fig. 7. Measured angular difference between the float on liquid's surface and the container during the transition from $\boldsymbol{o}_{0,0}^l$ to $\boldsymbol{o}_{0,1}^l$ using the feedforward control (blue) and without (red). Motion starts at $t_0 = 0.25\,\mathrm{s}$ and finishes at $t_1 \approx 2.4\,\mathrm{s}$.

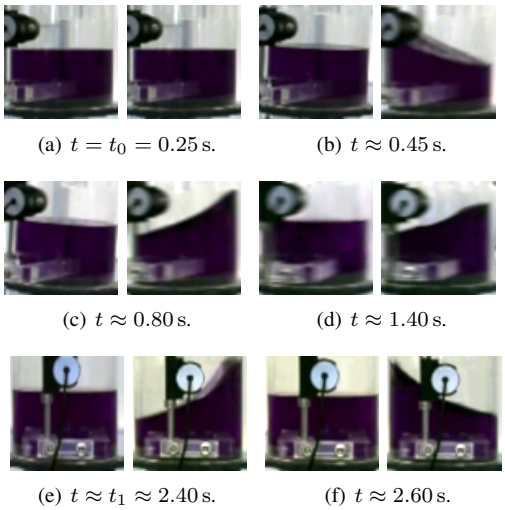

Fig. 8. Snapshots of the motion of the liquid filled container during transfer analogous to Fig. 7. In each subfigure the left-hand side photo illustrates the result with the proposed feedforward control while the right-hand side photo illustrates the sloshing with classical translational trajectory planning.

optimization-based trajectory planning and feedforward control approach and the classical translational approach. Snapshots of this video at different time instances are shown in Fig. 8. It can be seen that the angle between liquid surface and container reaches values up to approximately 45° without the feedforward control but, as expected from Fig. 7, remains at almost zero constantly with feedforward control.

Remark 1 (Measurement rate): Due to the rather low measurement rate of the used camera system and the subsequent image processing unit the sloshing amplitudes cannot be accurately determined at our present setup for fast angle changes. This explains the differences in the maximal values between Fig. 7 and Fig. 8.

B. Three-Dimensional Point-to-Point Motion With Obstacles

As described in Section III the optimization-based trajectory planning and feedforward control can be extended to consider obstacles in the environment of the planned path. This approach is simulated with six path points and two obstacles. At the path points the motion of the container is stopped. The resulting path is shown in Fig. 9 where the arrows depict the z_c-axis of the container frame. Due to the proposed extension of the objective functional (9) the planned trajectory passes the obstacles with a minimum distance but does not violate the obstacle limits. The manipulator accelerates after leaving a path point and decelerates before approaching the next one. It can be observed that during the acceleration phase the container is tilted in the direction of the path to compensate the sloshing of the liquid while it is tilted against the path direction while decelerating. During the curved motion the orientation of the container points inside the curvature of the path to compensate the centrifugal motion of the liquid.

Remark 2 (Experimental validation): During the tests of the proposed approaches an update of the robot manufacturer

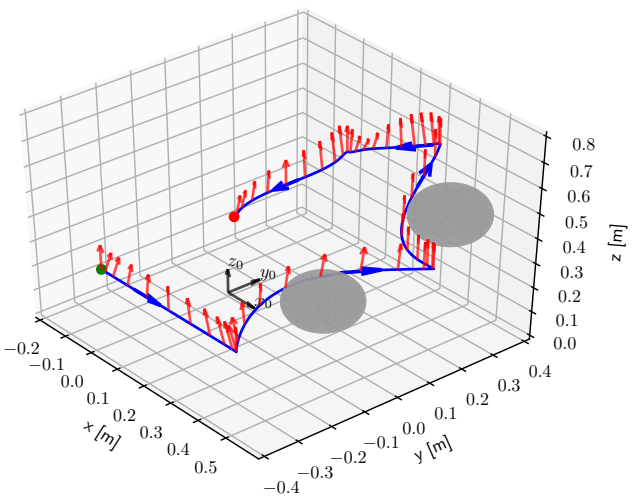

Fig. 9. Trajectory in three dimensional space with circuiting of obstacles. Arrows illustrate the orientation of the z_c-axis of the container.

Franka EMIKA GmbH has caused various malfunctions that prevent the external control of the robot to operate normally. As a result the experimental evaluation of scenario shown in Fig. 9 is not possible at the time of submission and a transfer to another robot model is underway.

V. CONCLUSION

This contribution proposes an optimization-based trajectory planning and feedforward control approach for the handling of liquid-filled container in three-dimensional space by using an industrial manipulator. The trajectory planning is realized by solving a constrained dynamic optimization problem considering the dynamic model of the liquid's sloshing motion. The experimental evaluations for one-dimensional motion trajectories confirm, that this approach enables us to completely suppress sloshing during point-to-point motion in minimal time. The extension to three-dimensional point-to-point trajectories involving obstacles is available and evaluated in simulation scenarios.

Ongoing work addresses the usage of a high speed camera to improve the image acquisition capabilities and thus to realize a combined optimization-based trajectory planning with vision-based feedback control to improve robustness.

ACKNOWLEDGMENT

The authors gratefully acknowledge the support by the project *InProReg*. *InProReg* is financed by Interreg Germany-Denmark with means from the European Regional Development Fund.

REFERENCES

[1] K. Yano and K. Terashima, "Robust liquid container transfer control for complete sloshing suppression," *IEEE Transactions on Control Systems Technology*, vol. 9, no. 3, pp. 483–493, May 2001.

[2] H. Sira-Ramirez, "A flatness based generalized PI control approach to liquid sloshing regulation in a moving container," in *Proceedings of the 2002 American Control Conference (IEEE Cat. No.CH37301)*, vol. 4, May 2002, pp. 2909–2914 vol.4.

[3] B. Bandyopadhyay, P. S. Gandhi, and S. Kurode, "Sliding mode observer based sliding mode controller for slosh-free motion through pid scheme," *IEEE Transactions on Industrial Electronics*, vol. 56, no. 9, pp. 3432–3442, Sep. 2009.

[4] M. Reyhanoglu and J. R. Hervas, "Point-to-point liquid container transfer via a PPR robot with sloshing suppression," in *2012 American Control Conference (ACC)*, June 2012, pp. 5490–5494.

[5] N. C. Singer and W. P. Seering, "Preshaping command inputs to reduce system vibration," in *Journal of Dynamic Systems, Measurement, and Control*, vol. 112, 1990, pp. 76–82.

[6] A. Aboel-Hassan, M. Arafa, and A. Nassef, "Design and optimization of input shapers for liquid slosh suppression," *Journal of Sound and Vibration*, vol. 320, no. 1, p. 1–15, 2009.

[7] W. Aribowo, T. Yamashita, K. Terashima, and H. Kitagawa, "Input shaping control to suppress sloshing on liquid container transfer using multi-joint robot arm," in *2010 IEEE/RSJ International Conference on Intelligent Robots and Systems*, Oct 2010, pp. 3489–3494.

[8] W. Aribowo, T. Yamashita, and K. Terashima, "Integrated trajectory planning and sloshing suppression for three-dimensional motion of liquid container transfer robot arm," *Journal of Robotics*, vol. 2015, Article ID 279460, p. 15, 2015.

[9] L. Moriello, L. Biagiotti, C. Melchiorri, and A. Paoli, "Control of liquid handling robotic systems: A feed-forward approach to suppress sloshing," in *2017 IEEE International Conference on Robotics and Automation (ICRA)*, May 2017, pp. 4286–4291.

[10] L. Biagiotti, D. Chiaravalli, L. Moriello, and C. Melchiorri, "A plug-in feed-forward control for sloshing suppression in robotic teleoperation tasks," in *2018 IEEE/RSJ International Conference on Intelligent Robots and Systems (IROS)*, Oct 2018, pp. 5855–5860.

[11] K. Terashima and K. Yano, "Sloshing analysis and suppression control of tilting-type automatic pouring machine," *Control Engineering Practice*, vol. 9, no. 6, p. 607–620, 2001.

[12] M. Hamaguchi, "Damping control of sloshing in liquid container in cart with active vibration reducer: The case of a curved path on a horizontal plane," *IEEE/ASME Transactions on Mechatronics*, vol. 24, no. 1, pp. 361–372, Feb 2019.

[13] R. Maderna, A. Casalino, A. M. Zanchettin, and P. Rocco, "Robotic handling of liquids with spilling avoidance: A constraint-based control approach," in *2018 IEEE International Conference on Robotics and Automation (ICRA)*, May 2018, pp. 7414–7420.

[14] B. Siciliano, L. Sciavicco, L. Villani, and G. Oriolo, *Robotics - Modelling, Planning and Control*. Berlin Heidelberg: Springer, 2009.

[15] R. A. Ibrahim, *Liquid Sloshing Dynamics: Theory and Applications*. Cambridge University Press, 2005.

[16] K. Yano and K. Terashima, "Sloshing suppression control of liquid transfer systems considering a 3-d transfer path," *IEEE/ASME Transactions on Mechatronics*, vol. 10, no. 1, pp. 8–16, Feb 2005.

[17] B. Houska, H. Ferreau, and M. Diehl, "ACADO Toolkit – An Open Source Framework for Automatic Control and Dynamic Optimization," *Optimal Control Applications and Methods*, vol. 32, no. 3, pp. 298–312, 2011.

[18] Franka EMIKA GmbH. (2017) Franka Control Interface (FCI). Infanteriestraße 19, 80797 München. [Online]. Available: https://frankaemika.github.io/docs/overview.html

[19] Kiel University, Chair of Automatic Control. (2019, Feb.) `acon_kiel_liquid_sloshing_supression.mp4`. Kaiserstrasse 2, 24143 Kiel. [Online]. Available: http://www.control.tf.uni-kiel.de/en/research/fileadmin/sloshing